Efficient temperature dependence of parameters for thermo-mechanical finite element modeling of Alloy 230

Hélène Morch[a, *], Laurent Duchêne[a], Ridha Harzallah[b], Víctor Tuninetti[c], Anne Marie Habraken[a,d]

[a] ArGEnCo Department, MSM team, University of Liège, Quartier POLYTECH 1, allée de la Découverte 9, Liège 4000, Belgium

[b] John Cockerill Energy, avenue Greiner 1, 4100 Seraing, Belgium

[c] Department of Mechanical Engineering, Universidad de La Frontera, Francisco Salazar 01145, Temuco 4780000, Chile

[d] Fonds de la Recherche Scientifique – F.N.R.S.–F.R.S., Belgium

---

Abstract

Nickel-based alloys are often selected for manufacturing components operating in extreme conditions such as high-temperature thermo-mechanical cyclic loadings because of their good corrosion and high temperature resistance. This is, for instance, the case for solar receivers where the material undergoes daily cycles going from ambient temperature to approximately 700°C. To predict the material behavior under this type of complex loadings, advanced numerical models – such as Chaboche-type models – are required. In addition to the model, a complete representation of the temperature dependency of the material is essential for both numerical stability and physical accuracy of the model, which is obtained with parameters assuring a certain continuity over the studied range of temperature. To this end, a new formulation for the temperature dependency of material parameters in Chaboche-type models is proposed for the Alloy 230 under both anisothermal and isothermal cyclic loadings.

Keywords: Alloy 230; Temperature dependency; Chaboche model; Constitutive model; Cyclic viscoplasticity; Thermo-mechanical fatigue

[*] Corresponding author:
E-mail address: helene.morch@uliege.be (H. Morch)

1. Introduction

The latest improvements in Concentrated Solar Power (CSP) technologies, and in particular the use of molten salt as a working fluid, have led to a significant increase in the levels of temperatures and stresses in these systems (Lata et al., 2008). The receiver of a CSP plant consists in a series of tubes made of nickel alloy inside of which flows a heat-transfer fluid (also called working fluid). As only one side of the tubes is exposed to solar radiation, the inhomogeneous temperature distribution in the cross-section of the tube leads to thermal stresses and deformations (Rodríguez Sanchez et al., 2013; Yang et al., 2012). The 700°C that the metal can reach on the exposed tube surface for several hours during the day causes creep deformation; meanwhile, the temperature variations during the day-night cycles lead to fatigue. Therefore, the tubes of the receiver are subjected to complex anisothermal cyclic loading with creep, and an advanced constitutive model is essential to accurately predict the behavior of the material under such complex loading.

Solar receivers are usually made of nickel alloys as these materials have excellent mechanical response at high temperature, including creep behavior (Morris et al., 2015) and corrosion resistance (Kruizenga et al., 2013; Liu et al., 2017; Novello et al., 2014). Alloy 230 was chosen owing to its superior corrosion resistance and thermal stability features in comparison to other alloys (Klarstrom, 2009).

In order to model the cyclic behavior of metals, several models have been developed over the years. The unified model developed by Chaboche et al. (1979) using the formulation of Frederick and Armstrong (2007) has been the basis for many other models (Chaboche, 2008). Notable improvements and developments include the addition of static recovery in the kinematic hardening rule (Chaboche, 1989), the introduction of a variable to represent the effect of the dislocation network formed under creep conditions by Yaguchi et al. (2002), and later the modeling of cyclic hardening through the kinematic hardening rule (Krishna et al., 2009). The Chaboche model is often used for the modeling of cyclic behavior (Bondar et al., 2018; Khutia et al., 2015; Zhan and Tong, 2007; Zheng et al., 2019), viscoplastic behavior (Chen et al., 2017; Wang et al., 2017), as well as temperature-dependent problems (Ahmed and Hassan, 2017; Cailletaud et al., 2015). As part of the development programs to increase the performances and reliability of solar receivers, a new constitutive model based on the work of Ahmed and Hassan, (2017) is developed for

nickel-based Alloy 230. The use of the material model will lead to an optimized solar receiver design with an accurate lifetime prediction applied in the present and the next generations of CSP tower technology.

This type of unified constitutive law with multiple optional features is very powerful for modeling complex behavior, however the drawback of using such complex models is the significant number of parameters. In addition, the solution to the identification problem is generally not unique for a given set of experiments. Because the parameters are temperature-dependent, the lack of uniqueness can have great impact when trying to fit the model for several temperatures independently. Indeed, as shown by Hosseini et al. (2015), the sets of parameters identified independently for each testing temperature led to a non-monotonous evolution of each parameter value with the temperature. It is therefore difficult to ascertain the validity of the model between two testing temperatures. Moreover, scattered parameters can lead to convergence problems when simulating anisothermal loadings. To avoid this problem, some researchers chose to express the parameters as polynomial (Yaguchi et al., 2002) or exponential (Desmorat and Otin, 2008; Ohno et al., 1989) functions of temperature after the identification. However, this approach is not always possible, especially when the identified parameters are very scattered. Considering this issue, Hosseini et al. (2015) proposed to fixate the temperature-dependent formulation prior to identifying the parameters. This method proved efficient for modeling the isothermal behavior of a 10% Cr steel under low cycle fatigue (LCF) conditions and dwell fatigue at mid-life, using a Chaboche model with 3 back-stresses for kinematic hardening.

The present study aims at expanding the use of Hosseini's formulation to anisothermal loading conditions and to the description of the behavior on the overall life of a sample of Alloy 230 subjected to a cyclic loading. While their study showed that their parameter formulation has proved to be efficient for modeling the increasing importance of creep with temperature, the formulation needs to be improved to model effects that are not monotonous with temperature. A slightly modified version of the model developed by Ahmed and Hassan (2017) for thermo-mechanical fatigue-creep of nickel-based Alloy 230 is used in this study to simulate the behavior of this material under complex thermo-mechanical loadings.

The outline of this article is as follows: Section 2 details the constitutive model to describe the behavior of Alloy 230 and the several methods available to determine the model parameters as a function of temperature

are explored in Section 3. The identification of the model parameters with the selected method for the appropriate range of temperature is explained in details in Section 4. The results of the modeling of cyclic hardening and the anisothermal loading are presented and analyzed in Section 5. Finally, the summary of the main conclusions is presented in Section 6.

2. Unified viscoplastic constitutive model

The constitutive model implemented in Lagamine finite element software ('Lagamine code') for this study was originally developed by Ahmed and Hassan, (2017). It is based on a previous isothermal version of the model (Ahmed et al., 2016) which derives from the Chaboche viscoplastic constitutive model framework (Chaboche, 2008).

2.1. Description

The main equations of the model are summarized hereafter. For clarity, the equations are only presented for the 1D case (scalar strain and stress).

The total strain is decomposed into thermal ε^{th}, elastic ε^{e}, and plastic ε^{p} strains, as expressed in Eq. (1):

$$\varepsilon = \varepsilon^{th} + \varepsilon^{e} + \varepsilon^{p} \quad (1)$$

The stress and the elastic strain are related through Hooke's law (Eq. (2)):

$$\sigma = E\varepsilon^{e} \quad (2)$$

The yield locus is defined using the von Mises criterion (Eq. (3)), where X is the back-stress representing kinematic hardening, R is the isotropic hardening variable, and σ_y is the yield stress. The evolution of the isotropic hardening variable is defined by Eq. (4), where Q is the saturated value of isotropic hardening, b its rate of evolution and p is the accumulated plastic strain defined by Eq. (5).

$$|\sigma - X| - R - \sigma_y \leq 0 \quad (3)$$

$$R = Q(1 - \exp(-bp)) \quad (4)$$

$$p = \int |\dot{\varepsilon}^{p}| dt \quad (5)$$

The kinematic hardening related variable X is expressed in rate form as the sum of three back-stresses X_i (Eq. (6)) in order to accurately model the short term and long term evolution during the cyclic loading (Morch et al., 2018).

$$\dot{X} = \sum_{i=1}^{3} \dot{X}_i \tag{6}$$

The evolution of the three back-stresses is based on the nonlinear kinematic hardening rule of Chaboche (1989) shown in Eq. (7) with an additional term to take into account the effect of temperature variation (Ohno et al., 1989). C_i, γ_i, b_i and r_i are material parameters, T is the temperature. Note that the Chaboche (1989) hardening rule is similar to the one of Frederick and Armstrong, (2007) with an additional term for the representation of static recovery. The present study focuses on the behavior of nickel Alloy 230 in a temperature range of 24°C to 750°C. Barrett et al., (2016) showed that within this temperature range, this alloy shows little to no strain-rate dependence. As a consequence, the viscous behavior of the material is modeled through static recovery – 3rd term in the kinematic hardening rule – rather than using the Norton-Hoff equation.

The 2 first back-stresses X_1 and X_2 follow the modified kinematic hardening rule proposed by Yaguchi et al., (2002) presented in Eq. (8). This improved rule includes a variable Y_i that evolves according to Eq. (9), where $\alpha_{b,i}$ is the rate of evolution of Y_i and $Y_{st,i}$ controls the saturated value of Y_i. The variable Y_i allows to model the evolution of the cyclic mean stress under creep-fatigue loading conditions that results from the effect of the dislocation network.

$$\dot{X}_i = C_i \dot{\varepsilon}^p - \gamma_i X_i \dot{p} - b_i |X_i|^{r_i - 1} \dot{X}_i + \frac{1}{C_i} \frac{dC_i}{dT} \dot{T} X_i \tag{7}$$

$$\dot{X}_i = C_i \dot{\varepsilon}^p - \gamma_i (X_i - Y_i) \dot{p} - b_i |X_i|^{r_i - 1} \dot{X}_i + \frac{1}{C_i} \frac{dC_i}{dT} \dot{T} X_i \tag{8}$$

$$\dot{Y}_i = -\alpha_{b,i} \left(sign(X_i) Y_{st,i} + Y_i \right) |X_i|^{r_i} \tag{9}$$

Although cyclic hardening is usually modeled through the isotropic hardening rule, Ahmed et al. (2016) found that Alloy 230 shows negligible evolution of the yield surface size, concluding that for this alloy the isotropic hardening is not required. Cyclic hardening is therefore modeled through the evolution of the dynamic recovery parameter γ_i in the kinematic hardening rule, as proposed by Ahmed and Hassan (2017).

The parameter γ_i evolves from its initial value $\gamma_{i,init}$ to a saturated value γ_i^0 at a rate D_{γ_i} as shown in Eq. (10), therefore changing the amplitude of variation of the back-stress X_i. To model the cyclic hardening of Alloy 230, the variation of γ_i is applied to two back-stresses. The first back-stress X_1 controls the short-term cyclic hardening, with a high value of D_{γ_1}, while the second back-stress X_2 is responsible for long-term hardening, with a small value of D_{γ_2}.

The saturated value γ_i^0 is calculated as a function of 3 material parameters a_{γ_i}, b_{γ_i}, c_{γ_i} (Eq. (11)). The strain memory surface characterized by its radius q is used to model the strain-range dependence of the material (Chaboche et al., 1979).

$$\dot{\gamma}_i = D_{\gamma_i}(\gamma_i^0 - \gamma_i)\dot{p} \tag{10}$$

$$\gamma_i^0 = a_{\gamma_i} + b_{\gamma_i}\exp(-c_{\gamma_i}q) \tag{11}$$

The strain memory surface g_M is defined by Eqs. (12) to (14), where H is the Heaviside step function and η a material parameter representing the rate of evolution to a steady memory surface. The value of η is set to 0.5 for an instantaneous memorization.

$$g_M(\varepsilon^p - \zeta) = |\varepsilon^p - \zeta| - q \tag{12}$$

$$\dot{q} = \eta H(g_M)\, sign(\sigma - X)\, sign(\varepsilon^p - \zeta)\dot{p} \tag{13}$$

$$\dot{\zeta} = (1-\eta)H(g_M)sign(\varepsilon^p - \zeta)\dot{p} \tag{14}$$

2.2. Numerical implementation

The material law described above was implemented as a subroutine in the updated Lagrangian Finite Element software called Lagamine developed by the University of Liège to model forming processes since 1985. The code is focused on the development and the identification of laws based on multi-scale or phenomenological approaches. These rheological models predict the damage and rupture along forming processes as well as under static or fatigue loading.

The radial return mapping method is used to find the stress in each finite element: an elastic predictor is first calculated using Hooke's law; if the von Mises criterion is not met, a viscoplastic corrector is then

calculated. The plastic corrector is calculated by solving a system of non-linear equations derived from Eqs. (3), (4), (7)-(9) as proposed by Ahmed, (2013) using the Newton-Raphson algorithm.

3. Parameter formulation

To model the behavior of Alloy 230 tubes under thermo-mechanical loading, the model parameters must be identified for an appropriate range of temperature. Several methods are available to determine parameters at various temperatures. The most common and most straightforward method is to identify parameters at every temperature for which experimental data are available independently. For intermediate temperatures, parameters will then be interpolated between identified values, using linear (Maier et al., 2013; Wang et al., 2017; Zhou et al., 2015), polynomial (Yaguchi et al., 2002), or exponential (Desmorat and Otin, 2008; Ohno et al., 1989) functions. Another method is to define the parameters as mathematical functions of the temperature prior to the identification step, and then directly identify these functions coefficients (Hosseini et al., 2015).

3.1. Linear interpolation of parameters

As a first approach, the parameters are indeed identified for several temperatures separately. The choice of the interpolation function between two testing temperatures then depends on the shape of the curve defined by the identified parameters. Parameters C_2 and γ_2 identified at five temperatures are shown in Figure 1. Piecewise linear interpolation was chosen rather than polynomial or exponential as some parameters – for instance C_2 – show non-monotonous evolution, which makes it impossible to use exponential function. Moreover, some parameters, as γ_2, are constant at low temperatures and evolve at high temperatures, requiring the definition of several polynomial functions depending on the temperature range. Given the number of parameters, implementing specific polynomial functions depending on the temperature range for each parameter was considered too arduous and unnecessary.

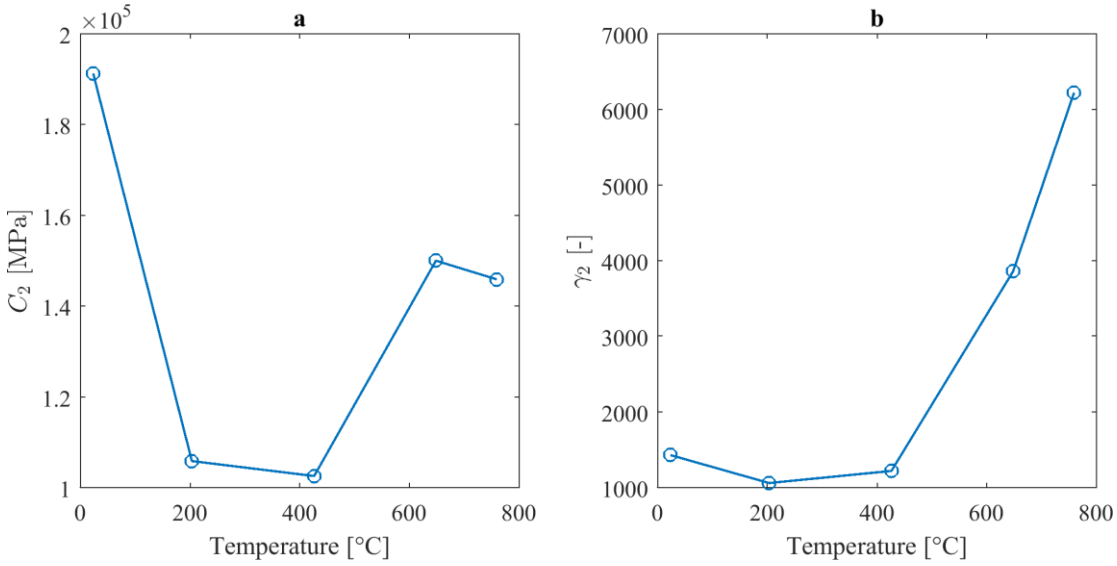

Figure 1 – Linear interpolation of parameters (a) C_2 and (b) γ_2 identified at five different temperatures independently

3.2. Exponential function

Due to the non-uniqueness of the solution of the identification problem at each temperature, identifying parameters independently for each temperature raises the problem of the validity of the model in-between the identification temperatures. As the value of each parameter only makes sense within the whole set of parameters, it is difficult to ascertain the validity of the sets of parameters obtained from linear interpolation. Hosseini et al., (2015) proposed a new formulation of the parameters as exponential functions of the temperature and showed that it gave good results for the representation of mid-life cycle of fatigue and creep-fatigue tests. This formulation described by Eq. (15), defines any P parameter of the Chaboche model as a function of the temperature T in Kelvin, A_P, B_P, C_P being the parameters associated to $P(T)$.

$$P = A_P\left(1 - B_P \exp\left(\frac{T}{C_P}\right)\right) \tag{15}$$

The parameters $B_{Ci}, B_{\gamma i}, B_{bi}$ and $C_{Ci}, C_{\gamma i}, C_{bi}$ related to the various back-stresses X_i are the same for every i. This choice is made for practical reasons, as it is impossible to differentiate the effect of temperature on each back-stress separately. The back-stresses do not have an actual physical meaning when taken separately, but using more than one back-stress improves the accuracy of the model, as observed by Benasciutti et al., (2018).

Exponent parameters $b, r_i, c_{\gamma i}$ are kept constant with temperature.

3.3. Double exponential

The formulation with a single exponential has one major drawback: the evolution of parameters with temperature is necessarily monotonous. It is the case for the majority of parameters, however, experimental results taken from Barrett et al., (2016) show that the cyclic hardening behavior of Alloy 230 is not monotonous with temperature. Long-term cyclic hardening, for instance, can be quantified as the difference between the stress amplitude at the end of the test and the stress amplitude after the saturation of the short-term hardening (around the 100th cycle for Alloy 230), as shown in Figure 2 (b) for LCF tests with a strain amplitude of 0.8% at different temperatures. It can be observed that Alloy 230 shows increasing amounts of cyclic hardening between 24°C and 427°C, but decreasing amounts of cyclic hardening between 649°C and 760°C. The high amount of cyclic hardening around 600°C can be explained by the significant precipitation of fine carbides at this temperature, while the decrease in hardening between 649°C and 760°C is due to the less dense carbide distribution at higher temperatures (Hasselqvist, 2002; Veverkova et al., 2008).

As mentioned before, cyclic hardening is modeled through the variation of parameters γ_1 and γ_2 towards their respective saturated value γ_1^0 and γ_2^0. When static recovery and evolution of mean stress can be neglected – this is the case for LCF tests – Eq. (8) can be integrated yielding to Eq. (16):

$$X_i = sign(\varepsilon^p)\frac{C_i}{\gamma_i}(1 - \exp(-\gamma_i|\varepsilon^p|)) \quad (16)$$

For an LCF test, considering that $\exp(-\gamma_i|\varepsilon^p|) \ll 1$ and combining Eq. (3) and (16), the stress amplitude can then be approximated by Eq. (17):

$$\sigma_{amp} \approx \sigma_y + R + \sum_{i=1}^{3}(C_i/\gamma_i) \quad (17)$$

From Eq. (17), knowing that R is almost constant for Alloy 230, it can be inferred that a value of $\gamma_i^0/\gamma_{i,init}$ larger than 1 induces negative hardening (softening), while for smaller values of $\gamma_i^0/\gamma_{i,init}$, hardening is significant. Considering the long-term cyclic hardening of Alloy 230, the value of $\gamma_2^0/\gamma_{2,init}$ should be above 1 for 24°C, decrease between 24°C and 427°C, and then increase between 649°C and 760°C.

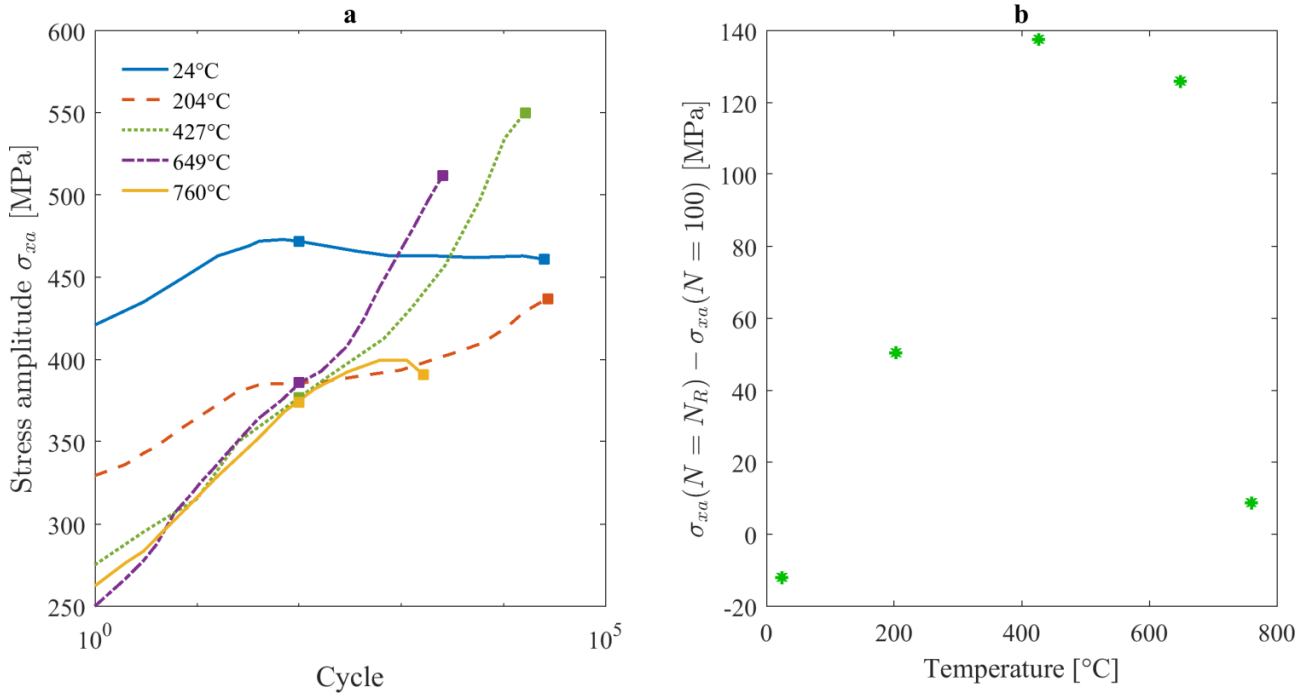

Figure 2- (a) Stress amplitude at different temperatures for a strain-controlled LCF test with 0.8% total strain amplitude from Barrett et al., (2016) with the 100th and the rupture cycles highlighted (b) Evolution of long-term cyclic hardening with temperature.

To take into account the variation in the cyclic hardening behavior of Alloy 230 with the temperature, the present study proposes a new formulation for cyclic hardening parameters $a_{\gamma_i}, b_{\gamma_i}$ and c_{γ_i} with the sum of two exponential functions and five temperature dependence parameters, as shown in Eq. (18):

$$P = \left(A_P\left(1 - B_P \exp\left(\frac{T}{C_P}\right)\right)\right) + \left(A_P\left(1 - D_P \exp\left(\frac{T}{E_P}\right)\right)\right) \quad (18)$$

Similarly to what was done in Section 3.2, the parameters B_P, C_P, D_P, E_P are considered identical for a_{γ_i} and b_{γ_i} for a given i, that is: $B_{a_{\gamma_i}} = B_{b_{\gamma_i}};\ C_{a_{\gamma_i}} = C_{b_{\gamma_i}};\ D_{a_{\gamma_i}} = D_{b_{\gamma_i}};\ E_{a_{\gamma_i}} = E_{b_{\gamma_i}}$ for $i \in [1,2]$. Introducing the formulation from Eq. (18) into Eq. (11) and considering $\exp(c_{\gamma_i} q) = K_q$ for a given q, parameter γ_i^0 can be written as shown in Eq. (19):

$$\gamma_i^0 = \underbrace{\left(A_{a_{\gamma_i}} + A_{b_{\gamma_i}} K_q\right)\left(1 - B_{a_{\gamma_i}} \exp\left(\frac{T}{C_{a_{\gamma_i}}}\right)\right)}_{P_1} + \underbrace{\left(A_{a_{\gamma_i}} + A_{b_{\gamma_i}} K_q\right)\left(1 - D_{a_{\gamma_i}} \exp\left(\frac{T}{E_{a_{\gamma_i}}}\right)\right)}_{P_2} \quad (19)$$

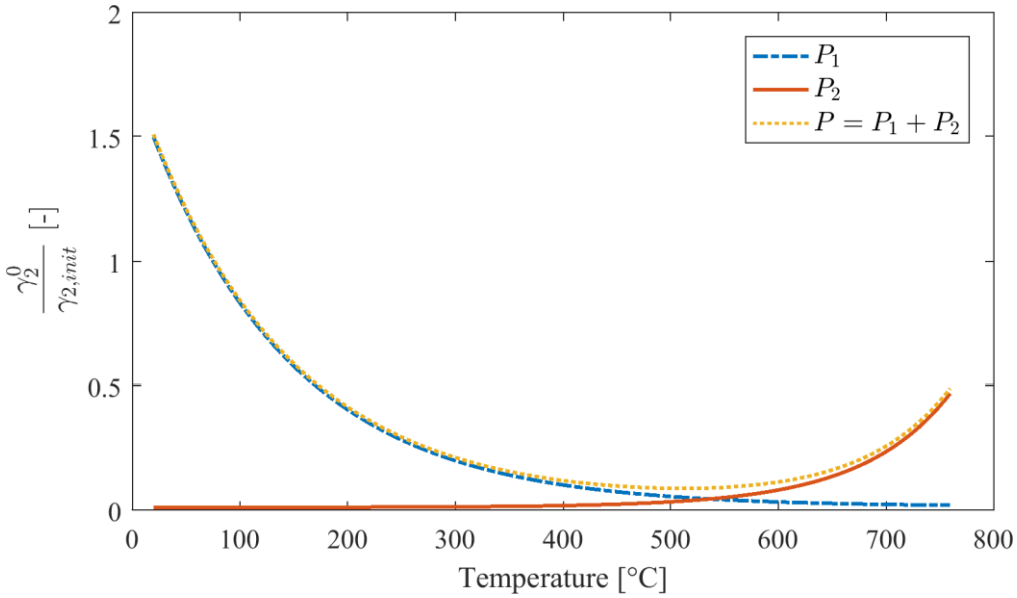

Figure 3- Double-exponential formulation of parameter γ_2^0 as a function of temperature, normalized with $\gamma_{2,init}$ parameter which is almost independent of T.

This new formulation allows a non-monotonous evolution of the parameters, as shown in Figure 3 where P_1 is the first term of Eq. (19) and P_2 is the second term. The initial value $\gamma_{2,init}$ is almost constant with temperature, which makes its influence on the shape of $\gamma_2^0/\gamma_{2,init}$ negligible. As expected from the analysis of Figure 2, the value of $\gamma_2^0/\gamma_{2,init}$ identified with the double-exponential formulation is above 1 at 24°C, decreases between 24°C and 427°C (increase of the cyclic hardening) and increases between 649°C and 760°C.

4. Parameter identification

For each formulation, the identification is performed in a two-step method:

- A first estimation of the parameters is found manually based on the experimental results from Barrett et al., (2016);
- The parameters are further optimized using the OPTIM code developed at the University of Liege based on the Levenberg-Marquardt algorithm and the implementation of the advanced model described in Section 2 within the home-made finite element code Lagamine ('Lagamine code')

The first estimation of the parameters was made for each temperature following the methods from Morch et al., (2018) and Tong et al., (2004). The parameters of the exponential formulations were computed using the

Excel solver to fit the exponential functions with the set of parameters identified at each temperature separately.

The optimization of the parameters was done sequentially, similarly to the methods proposed by Huang et al., (2014) and Zhan and Tong, (2007). The parameters are separated in different groups, each corresponding to a set of experimental results, to facilitate their identification. The groups are as follows:

- The elastic parameters E and σ_y are identified directly from the shape of the hysteresis loop on the first cycle of LCF tests – these parameters are not optimized;
- The isotropic hardening parameters b and Q are identified directly from the increase of the linear domain between the hysteresis loops of the first and the last cycles of LCF tests – these parameters are not optimized;
- The parameters for kinematic hardening and static recovery C_i, γ_i, b_i and r_i are identified from the hysteresis loops of the first cycle of LCF tests and creep-fatigue tests – the first cycle is considered to avoid effects from cyclic hardening;
- The parameters for cyclic hardening $D_{\gamma i}, a_{\gamma i}, b_{\gamma i}$ and $c_{\gamma i}$ are identified from the evolution of the stress amplitude of LCF tests;
- The parameters for mean stress evolution $Y_{st,i}$ and α_{bi} are identified from the evolution of the mean stress in creep-fatigue tests.

The normalized values of γ_1^0 and γ_2^0 calculated from the three different parameter formulations using Eq. (11) for a plastic strain radius $q = 0.26\%$ are shown in Figure 4. These two parameters control respectively short-term and long-term cyclic hardening. The values obtained with the three formulations are significantly different, because each parameter only makes sense as part of a set of parameters. However, it can be observed that both exponential formulations give close values. The double-exponential formulation allows a non-monotonous evolution of the parameters, giving a similar tendency to the parameters identified separately for each temperature (dots of the linear interpolation).

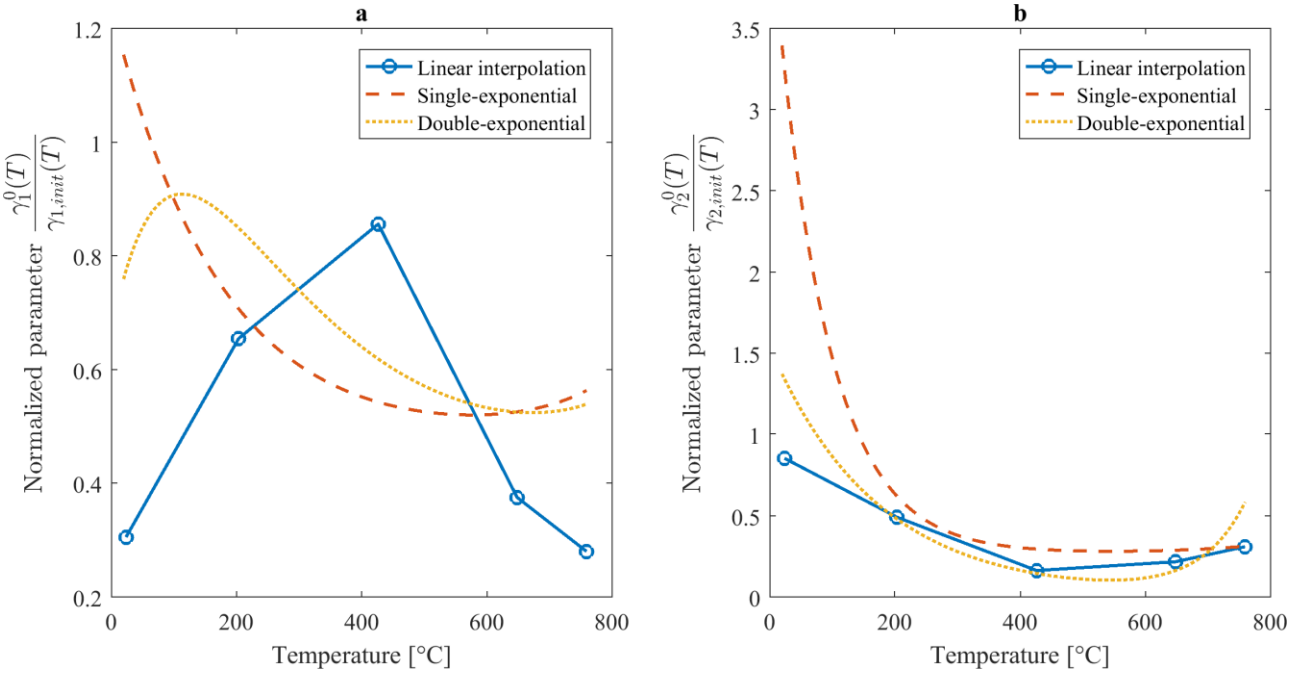

Figure 4 – Normalized values of (a) γ_1^0 and (b) γ_2^0 as functions of the temperature obtained from the three different parameter formulations for a plastic strain radius $q = 0.26\%$.

Regarding the total number of parameters of the model, it can be noted that the use of the exponential formulation reduces the total number of parameters in most cases. Indeed, for each testing temperature (five in our study) taken separately, there are 28 parameters to be determined: the Young modulus E, the yield stress σ_y, the isotropic hardening parameters b and Q, the kinematic hardening parameters $3 * (C_i, \gamma_i, b_i, r_i)$, the cyclic hardening parameters $2 * (D_{\gamma i}, a_{\gamma i}, b_{\gamma i}, c_{\gamma i})$, and the parameters describing the evolution of the mean stress $2 * (\alpha_{b,i}, Y_{st,i})$. Considering $b, r_i, c_{\gamma i}$ constant with temperature, the total number of parameters is therefore $N_{par}^{lin} = 6 + 22 * N_{temp}$, where N_{temp} is the number of testing temperatures for which parameters must be determined. This makes $N_{par}^{lin} = 116$. Considering now the exponential formulation with the double-exponential formulation for the cyclic hardening parameters: $a_{\gamma i}, b_{\gamma i}$ and the single-exponential formulation for the rest of the parameters (as they show a monotonous evolution with T), the total number of parameters is reduced to $N_{par}^{\exp} = 60$:

- 3 for each of E, σ_y, Q (9 in total);
- 1 for each exponent b, r_i $(i = 1{:}3), c_{\gamma i}$ $(i = 1{:}2)$ (6 in total);
- 2 for C_i, b_i, γ_i $\forall i$ (6 in total) and 1 for each $C_i, b_i, \gamma_i, i = 1{:}3$ (9 in total);
- 3 for each $D_{\gamma_i}, \alpha_{b,i}, Y_{st,i}$ $(i = 1{:}2)$ (18 in total);

- 1 for each cyclic hardening parameter $a_{\gamma i}, b_{\gamma i}$ $(i = 1{:}\,2)$ and 4 for every $i = 1{:}\,2$ (12 in total).

In general, $N_{par}^{\exp} < N_{par}^{lin}$ is verified as long as $N_{temp} \geq 3$. Even though the expression of parameters as functions of temperature may seem to make the model more complex, it actually lowers the total number of parameters to identify in the cases where there are more than two available testing temperatures.

5. Results

5.1. Thermo-mechanical simulation

To test the model with the exponential formulation, a thermo-mechanical simulation is conducted. In order to verify the validity of the model, an existing case study is chosen from Logie et al., (2018). The test consists in a tube from a solar receiver being exposed on one side to a solar flux $q''_{int} = 850$ kW/m² while a heat transfer fluid flows inside the tube at a constant temperature $T_{htf} = 450$°C. Due to the symmetry of the problem, only half of the tube is modeled, as shown in Figure 5 (a). A slice of tube of 0.2 mm thickness is modeled. The back of the tube (corresponding to $\theta = 180°$) is fixed and the upper and lower faces of the tube slice are made to remain parallel to account for the inability of the tube to be distorted. The non-uniform temperature distribution in the tube created by the solar flux is shown in Figure 5 (b) and (d). This non-uniformity combined with the fixations of the tube generates deformations and stresses in the tube.

We use the tube geometry and thermal properties of the salt (heat transfer fluid) described in Logie et al., (2018). However, in our case we chose to use material parameters corresponding to Alloy 230, as this material is the subject of this study and the identification of parameters for UNS S316000 would require comprehensive experimental data. Moreover, the model used here is a viscoplastic model, whereas Logie et al., (2018) used a thermoelastic calculation. The values of stresses are therefore not the same in Figure 5 (c) and (e), however the stress distribution is similar for both cases, with the maximum stress at the front of the tube, a quasi-uniform stress on the back of the tube (θ between 90° and 180°), and the minimum stress achieved in the quadrant between 45° and 90°. The comparison of both cases shows that our model is efficient for this type of thermo-mechanical problems.

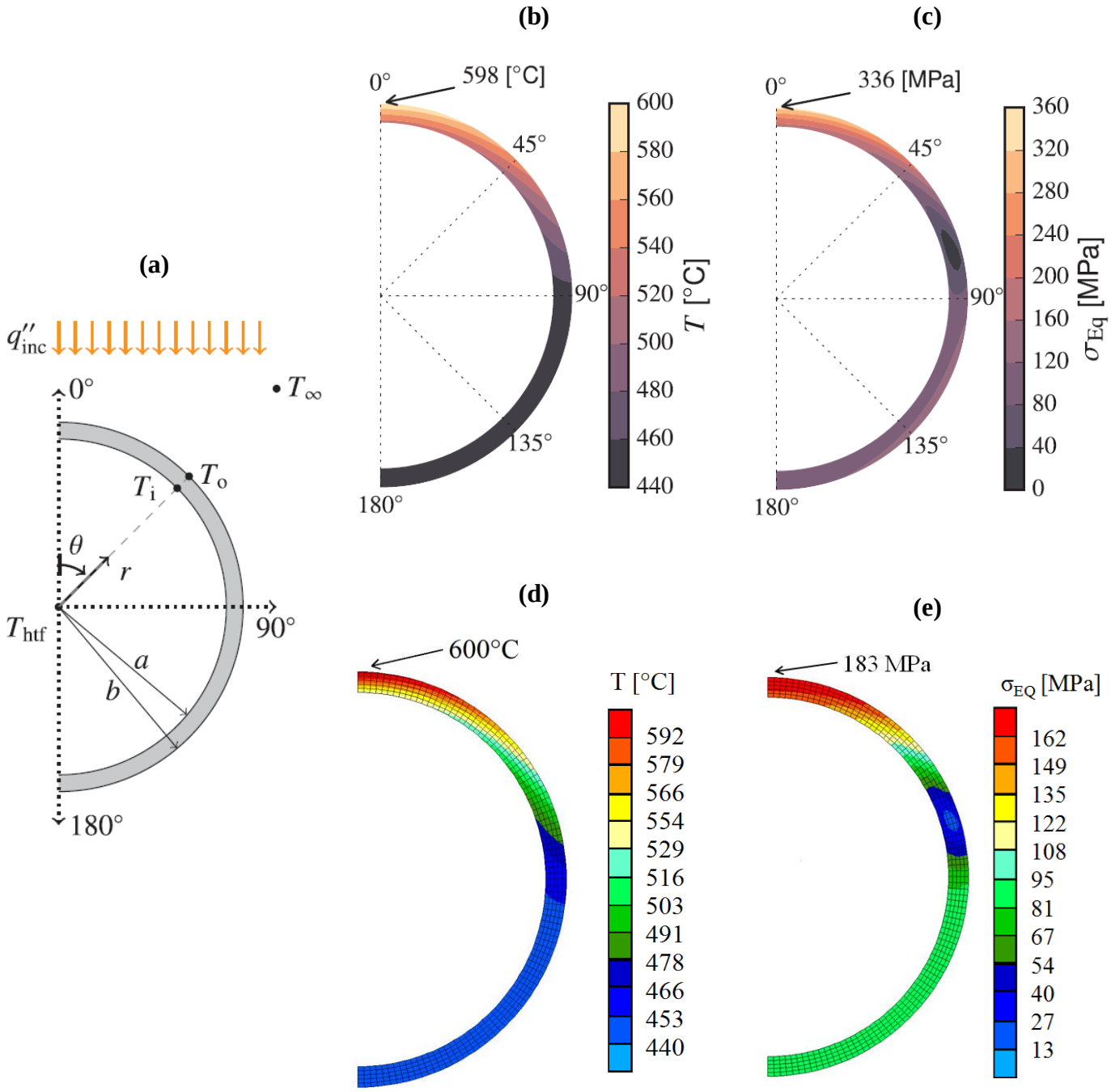

Figure 5 – Thermo-mechanical simulation of a solar receiver tube: (a) cross-section and heat loading, (b) temperature field, (c) von Mises stress distribution for UNS S31600 tubes from Logie et al., (2018) obtained using a thermoelastic model; (d) temperature field and (e) von Mises stress distribution for Alloy 230 tubes obtained using the thermo-mechanical model.

5.2. Anisothermal loading

The use of linear interpolation of parameters often leads to convergence problems when performing anisothermal simulations. Indeed, the discontinuity of the derivative of the parameters with respect to the temperature often induces issues around temperatures presenting strong parameter value peaks. However,

this problem can be resolved simply by selecting a function of class C^1 to describe the parameter evolution with the temperature.

The single-exponential formulation is compared to the linear interpolation for a cyclic anisothermal test taken from Ahmed et al., (2017). The loading, shown in Figure 6-(a), is a strain-controlled out-of-phase loading where the mechanical strain decreases while the temperature increases. The imposed strain is the total strain ($\varepsilon = \varepsilon^{mec} + \varepsilon^{th}$). The thermal strain ε^{th} is calculated using Eq. (20) where α is the coefficient of thermal expansion:

$$\varepsilon^{th} = \alpha \Delta T \tag{20}$$

Figure 6-(a) shows both the imposed thermal and mechanical cycles. During the 75 seconds of loading (heating) phase, the temperature increases from 316°C to 816°C, while the mechanical strain reaches 0.4% in compression. The first stage is followed by a holding time of 120 seconds during which the strain and temperature are constant. Finally, the last stage of the cycle consists of an unloading (cooling) phase of 90 seconds where the temperature and strain return to their initial values.

The first cycle of the anisothermal test was simulated using either the linear interpolation of the parameters or the single-exponential formulation. The double-exponential formulation was not used because it only concerns cyclic hardening, which does not appear in the first cycle. The simulations were performed for different values of time step (0.5s, 1s and 10s) to check the sensitivity of the integration scheme to the step size. The parameters for the linear interpolation were identified at 204°C, 427°C, 649°C, 760°C, and 871°C. The results of the simulations show that despite having very different values of parameters for the linear interpolation and the exponential formulation, the simulations give comparable results (Figure 6 (b), (c) and (d)).

The linear interpolation of parameters gives different results depending on the time step used for the simulation. Figure 6-(b) shows the results obtained for the simulation with a small time step of 0.5 s. The simulation stopped after reaching the temperature of 649°C due to convergence issues. Moreover, a discontinuity of the stress-strain curve is observed just before stopping. A similar discontinuity can be observed in Figure 6 (c), where the time step is 1s. However, the latter simulation was carried out to the end.

Finally, the discontinuity for a time step of 10s is much smaller (Figure 6-(d)). Convergence issues seem to arise more easily with smaller time steps. In the present case, the problem takes place around the temperature of 649°C. A possible explanation for this phenomenon is that one or several parameters reach a peak at 649°C. This is the case for instance for parameter γ_2, as shown in Figure 7. When the time step is small, the parameter is calculated around and at the peak, creating a strong discontinuity in the model – the parameter suddenly goes from a sharp increase to a steep decrease as can be seen for time steps of 0.5s and 1s. However, for larger values of the time step, the values of the parameter are calculated further away from the peak, as a consequence the change of behavior of the material is smoothened as the model ignores the strong discontinuity. This explanation is confirmed by the fact that the model does not converge with a time step of 1s when it is forced to pass at the time step corresponding to a temperature of exactly 649°C. The simulations performed using the exponential formulation give the same results whatever the time step and no discontinuity appears in the hysteresis loop.

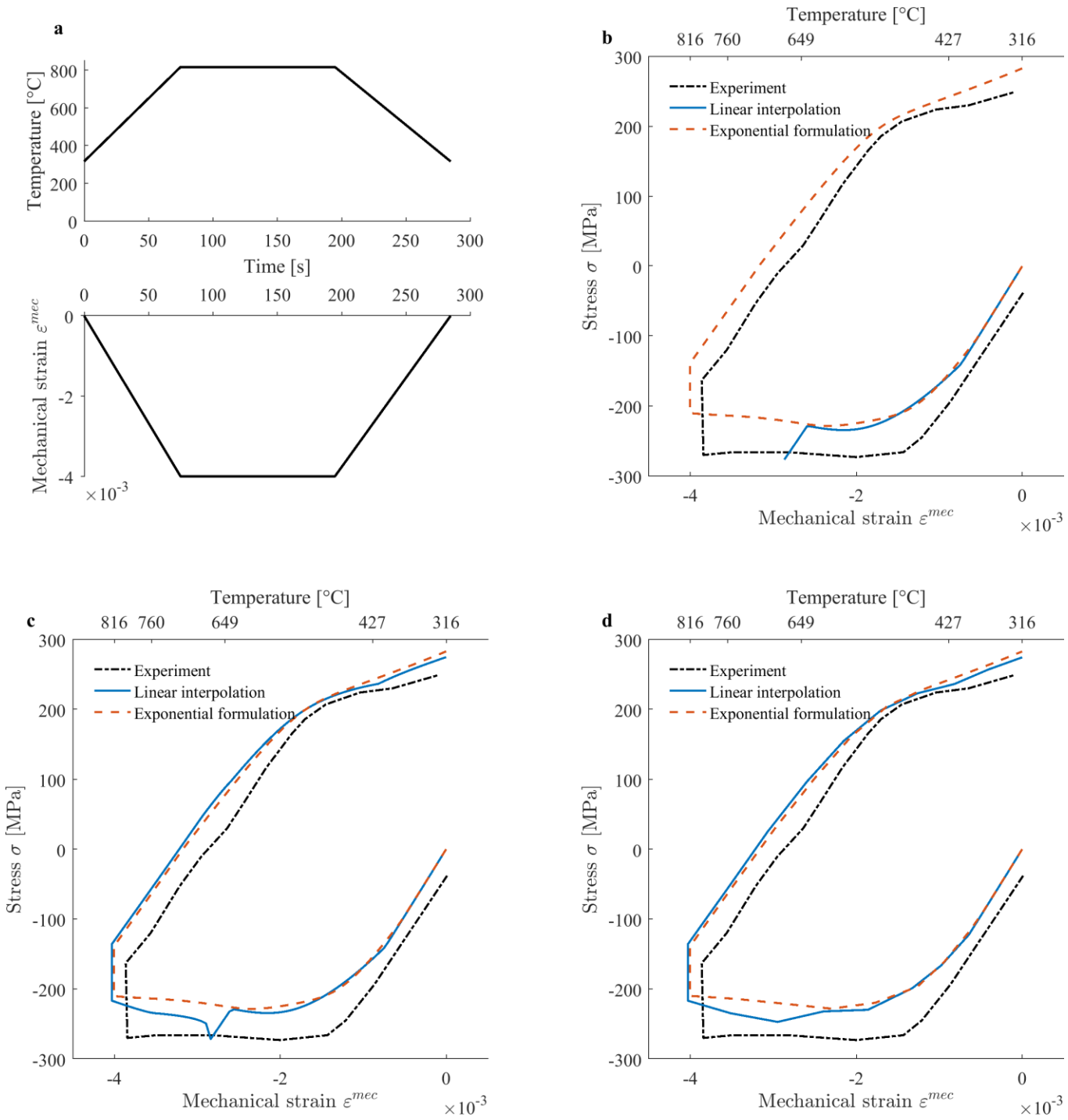

Figure 6 - Anisothermal results: (a) thermal and mechanical loadings;

hysteresis loops for the 1st cycle showing a comparison between experiments and simulations performed

with three time steps: (b) $\Delta t = 0.5\ s$ (c) $\Delta t = 1\ s$ (d) $\Delta t = 10\ s$.

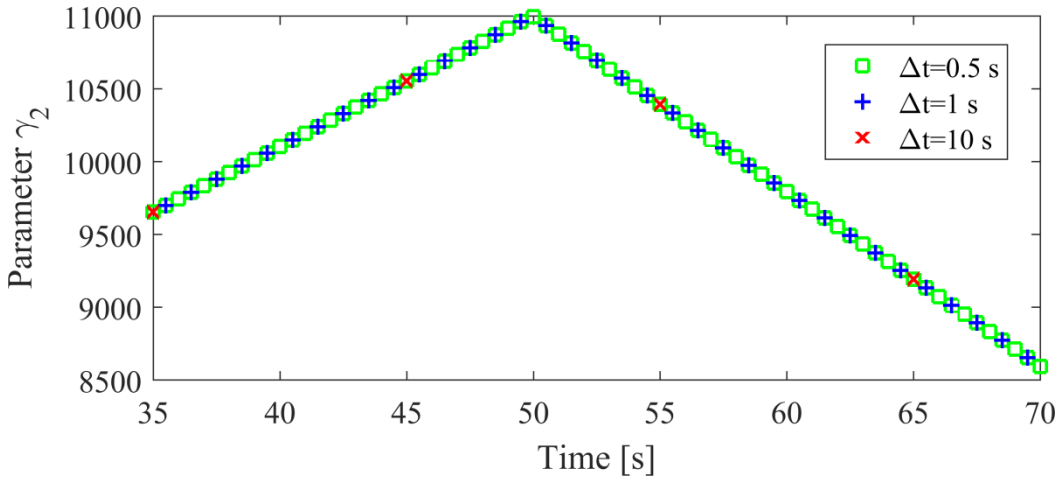

Figure 7 - Evolution of parameter γ_2 in the numerical simulation for different time steps

5.3. Cyclic hardening

As presented in Section 3.3, the cyclic hardening behavior of Alloy 230 changes non-monotonously with the temperature. The stress amplitude of low-cycle-fatigue tests for a strain amplitude of $\Delta\varepsilon = 0.8\%$ at different temperatures performed by Barrett et al., (2016) are compared with the simulations in Figure 8.

By identifying parameters at each testing temperature separately, the different cyclic hardening curves can be reproduced with sufficient accuracy. However, the result in between those temperatures is highly uncertain. Moreover, the simulations of anisothermal cyclic loadings such as the one described above are often stopped prematurely due to convergence problems.

The single-exponential formulation proved to be efficient to solve the continuity problem in anisothermal simulations, however it is limited to parameters evolving in a monotonous way with temperature. When used on parameters representing cyclic hardening, the single-exponential formulation does not yield good results for all temperatures, as can be seen in Figure 8. In particular, the long-term cyclic hardening is underestimated at temperatures of 24°C, 427°C, and 649°C, while it is over-estimated at 760°C. This can be a major issue when trying to estimate the lifetime of the material under a specific loading; if the stress is not estimated properly, the lifetime may be over or under-estimated as well. Simulations were performed using the cyclic hardening parameters identified with the double-exponential formulation – the rest of the parameters follow the single-exponential formulation. As can be seen in Figure 8, the results with this new formulation are very close to the experimental results, and bring a significant improvement compared with the single-exponential formulation.

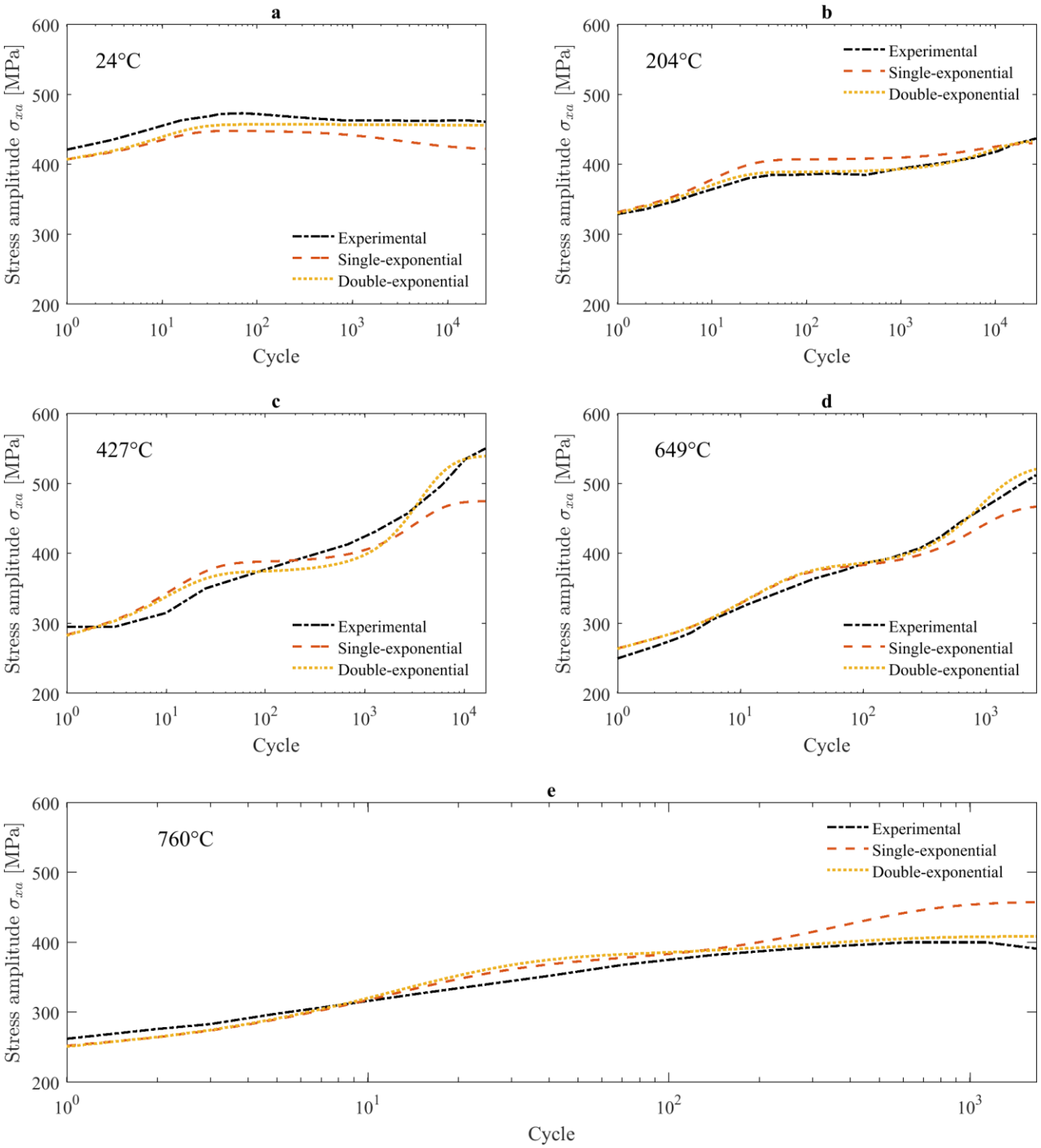

Figure 8 - Stress amplitude for strain-controlled LCF tests with Δε=0.8% at (a) 24°C (b) 204°C (c) 427°C (d) 649°C (e) 760°C.

Although using double-exponential formulation increases the number of parameters to be identified (5 parameters for double-exponential versus 3 parameters for single-exponential), it significantly improves the accuracy of the model. Moreover, the double-exponential is only necessary for a restrained number of

parameters (cyclic hardening parameters $a_{\gamma_i}, b_{\gamma_i}, i = 1{:}2$), hence the total number of parameters only increases by 4 (60 versus 56 in total).

6. Conclusion

Modeling the temperature dependence of material behavior, and more particularly the behavior under anisothermal loading is challenging and arduous. On the one hand, the behavior of Alloy 230 varies significantly with the temperature and a complex model is required to properly reproduce this behavior. On the other hand, a complex model requires more parameters, whose identification can be difficult and time-consuming. This is especially true when the material is studied over a wide range of temperatures rather than for one unique temperature. A good representation of the temperature dependence of the material parameters is the key to a well-functioning model, both in terms of physical accuracy and in terms of numerical efficiency.

In this study, the temperature dependence formulation proposed by Hosseini et al., (2015) was extended to anisothermal and cyclic behavior of Alloy 230. Their original formulation with parameters expressed as an exponential function of the temperature proved efficient in solving the continuity problem encountered with anisothermal loading when parameters are linearly interpolated between identified temperatures. However, a modification of the formulation was necessary for modeling the cyclic hardening which is not monotonous with temperature. The modified version with a double-exponential formulation proved very efficient in representing the cyclic hardening behavior at different temperatures.

Taking into account the temperature-dependence of material parameters prior to identification does not only improve the accuracy and convergence of the model, it also facilitates the identification process as the total number of parameters is reduced as long as the identification is made for more than two test temperatures.

Acknowledgements

The authors are grateful to John Cockerill Energy and to the Walloon Region for its financial support. The authors acknowledge the MecaTech Cluster and the Interuniversity Attraction Poles Program - Belgian State - Belgian Science Policy (P7-21). A.M. Habraken acknowledges the Belgian Fund for Scientific Research FRS-FNRS for its support. V. Tuninetti acknowledges the Chilean Scientific Research Fund Fondecyt 11170002 for its support.

References

Ahmed, R., 2013. Constitutive Modeling for Very High Temperature Thermo-Mechanical Fatigue Responses. North Carolina State University.

Ahmed, R., Barrett, P.R., Hassan, T., 2016. Unified viscoplasticity modeling for isothermal low-cycle fatigue and fatigue-creep stress-strain responses of Haynes 230. Int. J. Solids Struct. 88–89, 131–145. https://doi.org/10.1016/j.ijsolstr.2016.03.012

Ahmed, R., Barrett, P.R., Menon, M., Hassan, T., 2017. Thermo-mechanical low-cycle fatigue-creep of Haynes 230. Int. J. Solids Struct. 126–127, 90–104. https://doi.org/10.1016/j.ijsolstr.2017.07.033

Ahmed, R., Hassan, T., 2017. Constitutive modeling for thermo-mechanical low-cycle fatigue-creep stress-strain responses of Haynes 230. Int. J. Solids Struct. 126–127, 122–139. https://doi.org/10.1016/j.ijsolstr.2017.07.031

Barrett, P.R., Ahmed, R., Menon, M., Hassan, T., 2016. Isothermal low-cycle fatigue and fatigue-creep of Haynes 230. Int. J. Solids Struct. 88–89, 146–164. https://doi.org/10.1016/j.ijsolstr.2016.03.011

Benasciutti, D., Srnec Novak, J., Moro, L., De Bona, F., Stanojević, A., 2018. Experimental characterisation of a CuAg alloy for thermo-mechanical applications. Part 1: Identifying parameters of non-linear plasticity models. Fatigue Fract. Eng. Mater. Struct. 41, 1364–1377. https://doi.org/10.1111/ffe.12783

Bondar, V.S., Dansin, V. V., Vu, L.D., Duc, N.D., 2018. Constitutive modeling of cyclic plasticity deformation and low–high-cycle fatigue of stainless steel 304 in uniaxial stress state. Mech. Adv. Mater. Struct. 25, 1009–1017. https://doi.org/10.1080/15376494.2017.1342882

Cailletaud, G., Quilici, S., Azzouz, F., Chaboche, J.L., 2015. A dangerous use of the fading memory term for non linear kinematic models at variable temperature. Eur. J. Mech. A/Solids 54, 24–29. https://doi.org/10.1016/j.euromechsol.2015.06.007

Chaboche, J., 1989. Constitutive equations for cyclic plasticity and cyclic viscoplasticity. Int. J. Plast. 5, 247–302. https://doi.org/10.1016/0749-6419(89)90015-6

Chaboche, J.L., 2008. A review of some plasticity and viscoplasticity constitutive theories. Int. J. Plast. 24,

1642–1693. https://doi.org/10.1016/j.ijplas.2008.03.009

Chaboche, J.L., Dang Van, K., Cordier, G., 1979. Modelization of the Strain Memory Effect on the Cyclic Hardening of 316 Stainless Steel. SMiRT 5, Div. L.

Chen, W., Wang, F., Kitamura, T., Feng, M., 2017. A modified unified viscoplasticity model considering time-dependent kinematic hardening for stress relaxation with effect of loading history. Int. J. Mech. Sci. 133, 883–892. https://doi.org/10.1016/j.ijmecsci.2017.09.048

Desmorat, R., Otin, S., 2008. Cross-identification isotropic/anisotropic damage and application to anisothermal structural failure. Eng. Fract. Mech. 75, 3446–3463. https://doi.org/10.1016/j.engfracmech.2007.05.011

Frederick, C.O., Armstrong, P.J., 2007. A mathematical representation of the multiaxial Bauschinger effect. Mater. High Temp. 24, 1–26. https://doi.org/10.3184/096034007X207589

Hasselqvist, M., 2002. Viscoplastic Modelling for Industrial Gas Turbine (IGT) Application With Emphasis on the Sheet Material Haynes 230, in: Volume 3: Turbo Expo 2002, Parts A and B. ASME, Amsterdam, pp. 1229–1233. https://doi.org/10.1115/GT2002-30659

Hosseini, E., Holdsworth, S.R., Kühn, I., Mazza, E., 2015. Temperature dependent representation for Chaboche kinematic hardening model. Mater. High Temp. 32, 404–411. https://doi.org/10.1179/1878641314Y.0000000036

Huang, J., Shi, D.Q., Yang, X.G., Yu, H.C., Dong, C.L., 2014. Unified modeling of high temperature deformations of a Ni-based polycrystalline wrought superalloy under tension-compression, cyclic, creep and creep-fatigue loadings. Sci. China Technol. Sci. 58, 248–257. https://doi.org/10.1007/s11431-014-5679-x

Khutia, N., Dey, P.P., Hassan, T., 2015. An improved nonproportional cyclic plasticity model for multiaxial low-cycle fatigue and ratcheting responses of 304 stainless steel. Mech. Mater. 91, 12–25. https://doi.org/10.1016/j.mechmat.2015.05.011

Klarstrom, D.L., 2009. Haynes 230. Aerosp. High Perform. Alloy. Database.

Krishna, S., Hassan, T., Ben Naceur, I., Saï, K., Cailletaud, G., 2009. Macro versus micro-scale constitutive models in simulating proportional and nonproportional cyclic and ratcheting responses of stainless steel 304. Int. J. Plast. 25, 1910–1949. https://doi.org/10.1016/j.ijplas.2008.12.009

Kruizenga, A.M., Gill, D.D., Laford, M., Mcconohy, G., 2013. Corrosion of High Temperature Alloys in Solar Salt at 400, 500, and 680°C. Livermore, California.

Lagamine code, https://www.uee.uliege.be/cms/c_3680181/en/lagamine

Lata, J.M., Rodríguez, M., de Lara, M.A., 2008. High Flux Central Receivers of Molten Salts for the New Generation of Commercial Stand-Alone Solar Power Plants. J. Sol. Energy Eng. 130, 021002. https://doi.org/10.1115/1.2884576

Liu, B., Wei, X., Wang, W., Lu, J., Ding, J., 2017. Corrosion behavior of Ni-based alloys in molten NaCl-CaCl2-MgCl2eutectic salt for concentrating solar power. Sol. Energy Mater. Sol. Cells 170, 77–86. https://doi.org/10.1016/j.solmat.2017.05.050

Logie, W.R., Pye, J.D., Coventry, J., 2018. Thermoelastic stress in concentrating solar receiver tubes: A retrospect on stress analysis methodology, and comparison of salt and sodium. Sol. Energy 160, 368–379. https://doi.org/10.1016/j.solener.2017.12.003

Maier, G., Riedel, H., Nieweg, B., Somsen, C., Eggeler, G., Klöwer, J., Mohrmann, R., 2013. Cyclic deformation and lifetime of Alloy 617B during thermo-mechanical fatigue. Mater. High Temp. 30, 27–35. https://doi.org/10.3184/096034013X13636905345685

Morch, H., Duchene, L., Habraken, A.M., 2018. Identification method of an advanced constitutive law for nickel-based alloy Haynes 230 used in solar receivers. J. Phys. Conf. Ser. 1063. https://doi.org/10.1088/1742-6596/1063/1/012149

Morris, D.G., López-Delgado, A., Padilla, I., Muñoz-Morris, M.A., 2015. Selection of high temperature materials for concentrated solar power systems: Property maps and experiments. Sol. Energy 112, 246–258. https://doi.org/10.1016/j.solener.2014.09.050

Novello, F., Dedry, O., De Noose, V., Lecomte-Beckers, J., 2014. High Temperature Corrosion Resistance

of Metallic Materials in Harsh Conditions, in: Proceedings of the 10th Conference on Materials for Advanced Power Engineering 2014.

Ohno, N., Takahashi, Y., Kuwabara, K., 1989. Constitutive Modeling of Anisothermal Cyclic Plasticity of 304 Stainless Steel. J. Eng. Mater. Technol. 111, 106. https://doi.org/10.1115/1.3226424

Rodríguez Sanchez, M.R., Venegas Bernal, M., Marugán Cruz, C., Santana, D., 2013. Thermal, mechanical and hydrodynamic analysis to optimize the design of molten salt central receivers of solar tower power plants, in: International Conference on Renewable Energies and Power Quality. pp. 128–133. https://doi.org/10.24084/repqj11.238

Tong, J., Zhan, Z.L., Vermeulen, B., 2004. Modelling of cyclic plasticity and viscoplasticity of a nickel-based alloy using Chaboche constitutive equations. Int. J. Fatigue 26, 829–837. https://doi.org/10.1016/j.ijfatigue.2004.01.002

Veverkova, J., Strang, A., Marchant, G.R., Mccolvin, G.M., Atkinson, H. V, 2008. High Temperature Microstructural Degradation of Haynes Alloy 230. Superalloys 479–488. https://doi.org/10.7449/2008/Superalloys_2008_479_488

Wang, C., Shi, D., Yang, X., Li, S., Dong, C., 2017. An improved viscoplastic constitutive model and its application to creep behavior of turbine blade. Mater. Sci. Eng. A 707, 344–355. https://doi.org/10.1016/j.msea.2017.09.067

Yaguchi, M., Yamamoto, M., Ogata, T., 2002. A viscoplastic constitutive model for nickel-base superalloy, part 2: Modeling under anisothermal conditions. Int. J. Plast. 18, 1111–1131. https://doi.org/10.1016/S0749-6419(01)00030-4

Yang, Xiaoping, Yang, Xiaoxi, Ding, J., Shao, Y., Fan, H., 2012. Numerical simulation study on the heat transfer characteristics of the tube receiver of the solar thermal power tower. Appl. Energy 90, 142–147. https://doi.org/10.1016/j.apenergy.2011.07.006

Zhan, Z.L., Tong, J., 2007. A study of cyclic plasticity and viscoplasticity in a new nickel-based superalloy using unified constitutive equations. Part I: Evaluation and determination of material parameters. Mech.

Mater. 39, 64–72. https://doi.org/10.1016/j.mechmat.2006.01.005

Zheng, X., Wang, W., Guo, S., Xuan, F., 2019. Viscoplastic constitutive modelling of the ratchetting behavior of 35CrMo steel under cyclic uniaxial tensile loading with a wide range of stress amplitude. Eur. J. Mech. A/Solids 76, 312–320. https://doi.org/10.1016/j.euromechsol.2019.04.009

Zhou, C., Chen, Z., Lee, J.W., Lee, M.G., Wagoner, R.H., 2015. Implementation and application of a temperature-dependent Chaboche model. Int. J. Plast. 75, 121–140. https://doi.org/10.1016/j.ijplas.2015.03.002